Lattice Dynamics Signatures of Competing Orders in Unconventional Superconductors

S. M. Souliou, F. Weber & M. Le Tacon

Published online: 06 Sep 2023.

Submit your article to this journal ↗

View related articles ↗

View Crossmark data ↗

Lattice Dynamics Signatures of Competing Orders in Unconventional Superconductors

S. M. SOULIOU, ⓘ F. WEBER, ⓘ AND M. LE TACON ⓘ

Institute for Quantum Materials and Technologies, Karlsruhe Institute of Technology, D-76021, Karlsruhe, Germany

Introduction

Unconventional superconductivity typically refers to a superconducting state that stems from an effective attractive interaction between electronic quasiparticles, which is not the canonical electron-phonon coupling (EPC) [1]. The latter has been the key ingredient in unveiling the Cooper pairing mechanism on which builds the conventional theory of superconductivity (or theory of conventional superconductivity) originally proposed by Bardeen, Cooper, and Schrieffer [2].

The large variety of unconventional superconducting materials indicates that there is probably no unified theory of unconventional superconductivity that could account for all phenomena encountered in these materials. Nevertheless, it appears empirically that unconventional superconductivity often emerges in the neighborhood of closely degenerate electronic phases, which coexist, sometimes compete, or are even intertwined with the superconducting state [3, 4]. Critical fluctuations associated with these other electronic phases are often suspected to play a decisive role in unconventional superconducting pairing, which has in turn motivated the development of experimental tools allowing us to probe materials of interest at energies and momenta matched to their intrinsic collective responses.

As such, even though the EPC does not appear to be the primary driver of unconventional superconductivity, the coupling of electronic to lattice degrees of freedom has proven to be a sensitive probe of competing orders. Renormalization of the phonon spectra across electronic phase transitions is a particularly well-suited approach for these investigations. It has recently benefited a lot from the development of inelastic X-ray scattering (IXS) [5], which enables in particular the use of high pressures (in the tens of GPa range) as a "clean" way to drive a system across phase transitions.

In this short topical review, we illustrate this by reporting three recent cases in which phonon spectroscopy has been particularly insightful in addressing the physics of competing orders in unconventional superconductors, namely the high-temperature superconducting cuprates, Fe-based superconductors, and their Ni-based cousins.

Phonon spectroscopy in the cuprates: Stripe and CDW orders

The interplay between high-temperature superconductivity and various forms of charge/spin ordering in the cuprates has been widely debated in a vast literature [6], and the signature of this interplay in the lattice dynamics of these materials has been one of the pivotal arguments fueling this debate.

Anomalies in the dispersion or lifetime of high-energy optical phonon branches with symmetries compatible with in-plane modulations of the charge have been reported in essentially all families of hole and electron-doped cuprates ($YBa_2Cu_3O_{6+x}$ [7–10], $La_2(Sr/Ba)CuO_4$ [10, 11], $Bi_2Sr_{2-x}La_xCu_2O_6$ [12], $HgBa_2CuO_{4+d}$ [13], $Nd_{2-x}Ce_xCuO_{4+d}$ [14]) and, in the absence of evidence for static charge order, generally interpreted as fingerprints of fluctuating charge stripes [15, 16].

The more recent discovery of ubiquitous short-range, two-dimensional charge density waves (CDW) on the underdoped side of the phase diagram in essentially all cuprates families has sparked intense research activity [17–20]. The in-plane CDW correlation lengths are the largest in the LBCO and YBCO families, reaching 250 [21] and ~80 Å [22, 23], respectively, close to the 1/8 doping and in the absence of external magnetic field or pressure. Most naturally, the lattice dynamics in these systems has been revisited first. These investigations are best guided by first-principle calculations that can be used to identify potentially unstable phonon branches as well as the scattering geometry best suited to measure them (that is, the Brillouin zones in which the promising phonons have the largest structure factor).

In the case of cuprates, however, *ab initio* calculations have not identified CDW instabilities, making it hard to predict *a priori* which of the many phonon branches is best to focus on in the limited available beamtime slot [24, 25]. In order to guide these investigations, thermal diffuse scattering (TDS) mapping of the reciprocal space as a function of temperature constitutes a most valuable approach, which enables a rapid identification of regions of the reciprocal space where anomalous phonon softening (which gives rise to an increased TDS signal) might occur [26]. This is, for instance, illustrated for the case of YBCO in Figure 1(a), in which maps of the reciprocal (0KL) plane are shown at room temperature and 90K [25]. In the latter case, weak diffuse satellites corresponding to the CDW can be seen, albeit with strong intensity variations across the reciprocal space. IXS close to a strong satellite, such as that seen in the Brillouin zone centered around the (006) Bragg reflection, allowed the discovery of surprisingly strong anomalies of some of the low-lying acoustical and optical phonon branches around the incommensurate CDW wavevector Q_{CDW} [25, 27, 28, 30, 31].

More specifically, IXS investigation of the phonon dispersion across Q_{CDW} in these compounds revealed three distinct features,
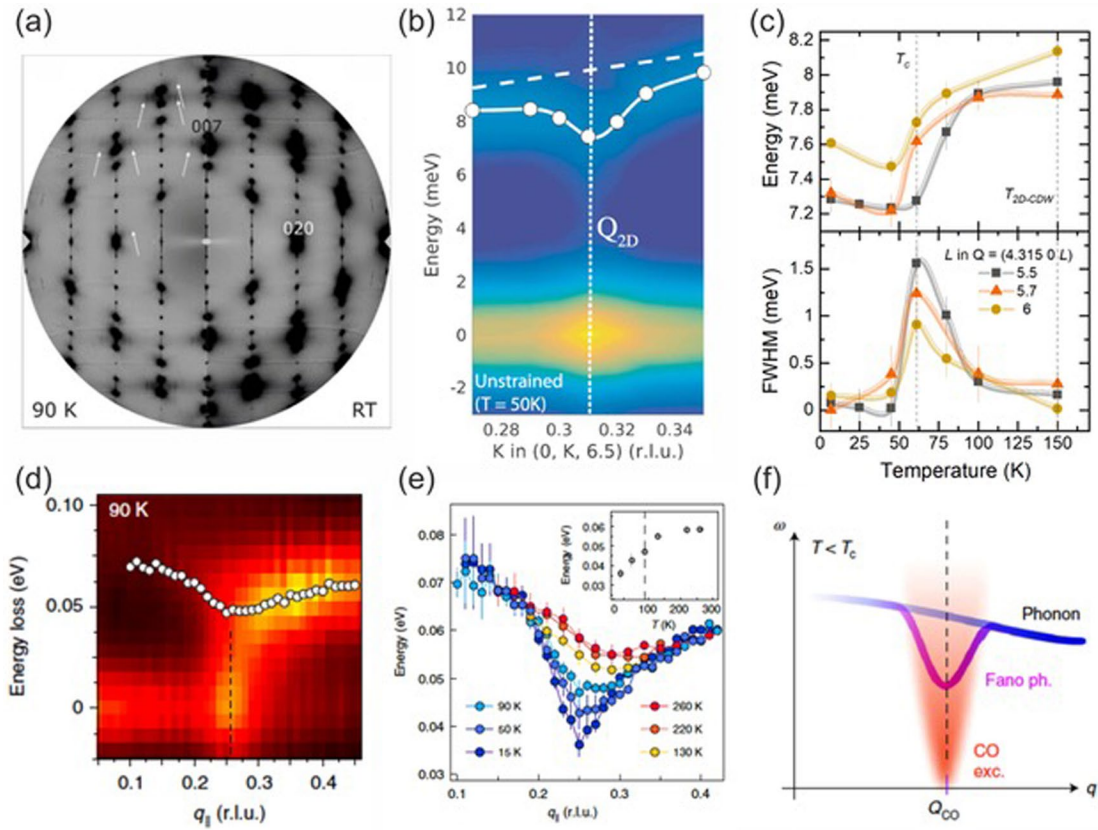
Figure 1: (a) The H0L plane of $YBa_2Cu_3O_{6.6}$ reconstructed from diffuse scattering data recorded at room temperature (right) and at 90 K (left). The white arrows indicate the CDW satellites. The figure is taken from reference [25]. (b) IXS intensity versus total momentum transfer recorded across Q_{CDW} in the 0KL plane of $YBa_2Cu_3O_{6.67}$ at $T < T_c$. The dashed line corresponds to the calculated dispersion, whereas the solid line is a guide-to-the-eye to the measured dispersion of the low energy acoustical phonon mode. From [27]. Reprinted with permission from AAAS. (c) Temperature dependence of the energy and linewidth of the B_1 acoustical phonon recorded at Q_{CDW} in the H0L plane of $YBa_2Cu_3O_{6.55}$. Reproduced from reference [28]. © 2021 The Physical Society of Japan. (d) RIXS intensity map recorded in nearly optimally doped $Bi_2Sr_2CaCu_2O_{8+}\delta$ at T_c (90 K) across the charge ordering wavevector (vertical black dashed line). (e) Temperature dependence of the fitted RIXS phonon dispersion. The inset shows the phonon energy at $q_{||} = 0.25\,r.l.u$ and the dashed line indicates the superconducting T_c. (f) A sketch of the model presented in [29], showing the phonon dispersion modified by Fano interference with the charge order excitation (the charge order excitation continuum is illustrated by the red shaded area, whereas the momentum dependence of the electron–bond-stretching phonon coupling strength is illustrated by the blue colour gradient). Panels (d, e, f) are reproduced with permission from [29].

namely (1) a sharp increase of the quasi-elastic line intensity at Q_{CDW} (Figure 1(b)), which increases below a temperature T_{CDW}, before eventually decreasing upon further cooling in the superconducting state below T_c (only seen in YBCO[25, 27, 28], T_c being too low in the investigated LBCO compounds [32]) (2) a broadening of the lowest energy phonon branches for temperatures down to T_c (Figure 1(c)); and (3) a steep softening and sharpening at Q_{CDW} at lower temperatures (Figures 1(b) and (c)). This phenomenology is very distinct from that encountered in classical soft-mode driven CDWs in low-dimensional metals [33–36], in which the softening of the phonon typically occurs above the CDW transition temperature. This, in turn, suggests an unusual interplay between superconductivity and CDW in these materials [37, 38]. Note that the behavior of the low-frequency phonons contrasts significantly with that of higher-energy branches, which exhibit

anomalies already at room temperature [16], at which only very short range CDW fluctuations have recently been detected [39].

It also is worth noting that the increase of the energy resolution of resonant inelastic (soft) X-ray scattering [40] has recently opened a new avenue for phonon spectroscopy [41, 42]. The method is only sensitive to those phonons that strongly couple to the electrons [43], providing a natural "filter" and enabling, in particular, a direct experimental determination of the electron-phonon coupling [44]. Direct evidence for a coupling between charge order fluctuations and high-energy bond-stretching phonons has been reported [45] (Figures 1(d)–(f)), and study of the renormalization of the resulting excitation through the superconducting transition has been interpreted as evidence for melting of the charge order through quantum critical fluctuations [29].

Hydrostatic pressure effects

The highest known superconducting critical temperatures have been recently reported in hydrides under very high pressures (Mbars) generated by means of diamond anvil cells (DAC) [46, 47]. While some of these results remain highly controversial, the idea of using pressure to explore the electronic phase diagram of conventional and unconventional superconductors is not new and is considered as a clean way (by opposition to chemical doping) to tune the balance between the different relevant interaction parameters in a solid. Using DACs, one can routinely access pressures of a few 10 GPa in the best hydrostatic conditions possible (using, e.g., helium as pressure medium), albeit with the drawback that the volume of materials that can be pressurized within is generally very small (typical sample sizes few 10 μm), which severely limits the possible experimental probes. On the other hand, DACs are compatible with photon scattering spectroscopies over a wide range of the electromagnetic spectrum, in particular in the visible and hard X-ray ranges, thereby allowing investigation of phonon dispersions using IXS under high pressure [48].

In underdoped YBCO, it has long been reported that hydrostatic pressurization can result—depending also on the exact doping level of the pressurized sample—in a strong increase of T_c that, in some cases, almost doubles by 15 GPa [49] (a recent review of the high-pressure effects on high-T_c cuprates is given in [50]). IXS measurements have recently shown that all signatures of the CDW in the low-energy phonon spectra of this compound, such as the mode broadening above T_c or the phonon softening, were suppressed with a relatively modest pressure of ~1 GPa (Figures 2 (a) and (b)) [31]. This suggests a very rapid suppression of the CDW as the superconducting phase is enhanced. This result nevertheless contrasts with other reports of the CDW surviving up to larger pressures from experiments carried out using different types of pressure cells and with different pressure transmitting media [51, 52].

Uniaxial pressure effects

An alternative approach to investigate the nature of the interplay between superconductivity and CDW in the cuprates consists in suppressing superconductivity. This can be achieved using either non-magnetic impurities or magnetic fields. Non-magnetic impurities such as Zn are strongly pair-breaking in nodal superconductors, and constitute a very efficient way to suppress T_c[53]. In the case of cuprates, they happen to also be detrimental to CDW and to promote instead incommensurate short-range magnetic orders [54]. A few Raman scattering [55, 56] and optical studies [57] have been reported, but to the best of our knowledge their impact on the lattice dynamics has not been investigated at finite momentum.

Magnetic fields are a more canonical way to suppress superconductivity, but cuprates exhibit very critical fields [58] and the realization of inelastic scattering experiments under magnetic fields sufficiently large to suppress superconductivity significantly (typically >10 T) has not taken place for technical reasons.

Building on early observations that the dependence of T_c to uniaxial pressure is highly anisotropic in the cuprates, an alternative route has recently been explored. In YBCO in particular, a-axis pressure can very effectively obliterate superconductivity [59, 60] and a compression of ~1% of the a lattice parameter of underdoped YBCO, amounting to ~1 GPa, can decrease T_c from ~65 to ~45 K [61]. Moreover, it was shown to strengthen the 2D CDW in the plane perpendicular to the applied strain [62]. For compression of ~0.8%, a 3D long-range-ordered CDW [27], which had been only reached otherwise using magnetic fields larger than ~15 T [63–67], is induced. Phonon spectroscopy then revealed that the transition to the 3D CDW appears driven by the softening of an optical phonon, which is strongly renormalized in the superconducting phase (Figures 2(c)–(d)) [27].

Iron-based superconductors: Phonons and nematic fluctuations

Superconductivity in many iron-based superconductors emerges when an antiferromagnetic spin-density-wave (SDW) ground state is suppressed either by doping or pressure [68] where the magnetic ordering is accompanied or preceded by a transition from a tetragonal (C_4) to orthorhombic (C_2) structure [69–72]. While it is generally assumed that the same type of fluctuations, termed nematic, are responsible for both magnetic and structural/nematic phase transitions in these compounds, the nematic phase without long-range magnetic order is only observed at temperatures $T_N < T < T_s$ in the latter type of iron pnictides [70, 73] and chalcogenides [74].

IXS experiments have been applied to iron-based superconductors [75–77] shortly after their discovery in 2008 [78]. Compared to oxygen bond-stretching phonons in cuprates, the relevant ions are heavy and, thus, make IXS much more favorable for phonon spectroscopy in iron-based superconductors. Early studies [79, 80] concluded that there are no strongly anomalous modes; e.g., having a large linewidth or a dispersion anomaly. However, comparison to *ab-initio* lattice dynamical calculations revealed that the agreement is generally improved for magnetic calculations, even when the compounds are in a non-magnetic state [81, 82]. On the other hand, measurements in the magnetic ground state (e.g., of the parent compounds) did not find the predicted splitting of the phonon modes in the orthorhombic structures [79, 82]. It is worth noting that large single crystals of Ba(Fe$_{1-x}$Co$_x$)$_2$As$_2$ became available relatively soon. Thus, inelastic neutron scattering was used to look for phonon anomalies on entering the superconducting phase at energies close to those of the superconducting energy gap 2Δ, but none were found [83].

More recently, the focus has shifted to investigations of the acoustic soft mode related to the onset of the nematic phase at T_s. IXS measurements reported the softening of the in-plane polarized transverse acoustic (TA) phonon mode propagating along the [010] direction (tetragonal notation) at the magnetic-structural phase transition in BaFe$_2$As$_2$ as early as 2011 [84], followed by a detailed neutron scattering study, including also SrFe$_2$As$_2$ [85]. The latter work emphasized a
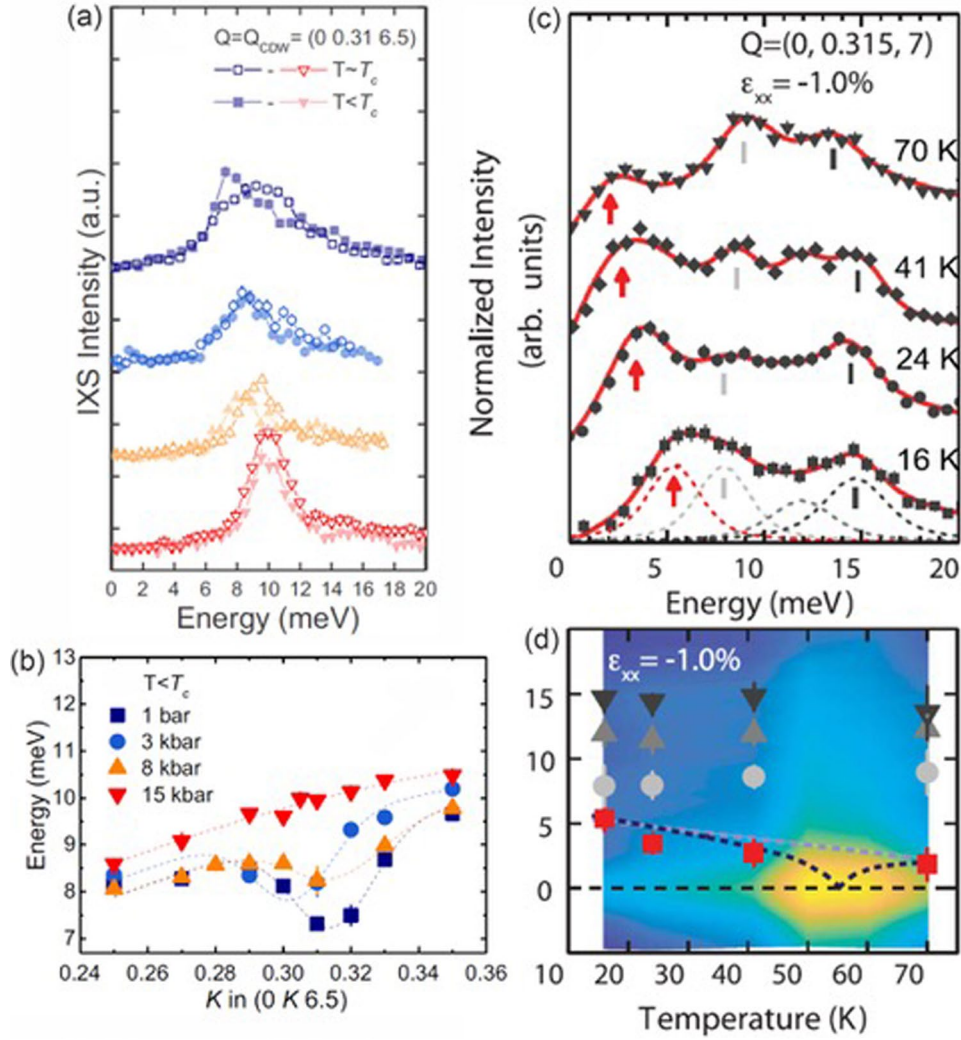
Figure 2: (a) Pressure dependence of the inelastic part of the IXS spectra of $YBa_2Cu_3O_{6.6}$ recorded at the CDW ordering wavevector at ~T_c (open symbols) and below T_c (solid symbols). Reprinted figure with permission from [31]. Copyright (2018) by the American Physical Society. (b) Pressure and momentum dependence of the renormalized acoustical phonon energy below T_c. Reprinted figure with permission from [31]. Copyright (2018) by the American Physical Society. (c) Temperature dependence of the inelastic part of the IXS phonon spectra of $YBa_2Cu_3O_{6.67}$ recorded at the 3D-CDW ordering wavevector under ε_{xx} ~ −1.0%. The soft phonon is indicated by the red arrow. From [27]. Reprinted with permission from AAAS. (d) Temperature dependence of the phonon energies recorded on $YBa_2Cu_3O_{6.67}$ at the 3D-CDW ordering wavevector under ε_{xx} ~ −1.0%. The color map depicts the measured IXS intensity (log scale). From [27]. Reprinted with permission from AAAS.

close correlation between magnetic properties, such as the size of the fluctuating magnetic domains above and the magnetic ordered moment below the magnetic-structural phase transition, and the softening and hardening of the TA phonon in the respective temperature ranges. Measurements extending these investigations to doped compounds found that the TA mode, in fact, responds primarily to nematic fluctuations rather than to the onset of magnetic order [86, 87]. Here, nematic order at $T_N < T < T_s$ triggers an orthorhombic distortion of the high-temperature tetragonal structure [88]. Even though, in this case, the lattice is not the driving force behind nematicity, it responds to nematic order and to nematic fluctuations due to the coupling to the electronic

degrees of freedom [89, 90]. In the paranematic phase with tetragonal symmetry at $T > T_s$, nematic fluctuations soften the shear modulus C_{66} due to the nemato-elastic coupling $\lambda \varphi \epsilon_{66}$ in the free energy.

The same coupling then yields the general relation $C_{66}(q) = C^0_{66} / (1 + \lambda^2 \chi_{nem}(q) / C^0_{66})$ between the renormalized elastic constant C_{66}, the bare elastic modulus C^0_{66} without nematicity, and the nematic susceptibility [91]. $C_{66} = C_{66}(q = 0)$ has been measured either directly by resonant ultrasound or indirectly via the Young's modulus Y_{110} in three-point bending setups [91–93]. For members of the 122 and 11 families of iron-based superconductors, $\sqrt{C_{66}}$ is, in the q=0 limit, proportional to the slope of the TA mode investigated already in

[84]. Taking into account the nemato-elastic coupling, the dispersion of this mode, renormalized by nematic fluctuations at T>T$_s$, can be described as [86]:

$$E(q) = f(q)\sqrt{[C^0_{66}(1+\xi^2 q^2)]/[\rho(C^0_{66}/C_{66}+\xi^2 q^2)]} \qquad (1)$$

where ρ is the density of the material. The function $f(q)$ is the unrenormalized dispersion, which must vanish linearly with q as $q \to 0$. Since the shear moduli were known for Ba(Fe$_{1-x}$Co$_x$)$_2$As$_2$ and FeSe [91–93], measurements of the phonon dispersion via IXS can be used to determine the nematic correlation length ξ as a function of temperature [87]. In the example shown in Figure 3(a), ξ corresponds to the wave vector at which the dispersion based on Eq. (1) (solid black line) bends upwards away from $\sqrt{C_{66}/\rho} \times q$ (dashed line). A power law fit for ξ versus temperature T of the form $\xi = \xi_0 / (T - T_0)^{1/2}$ (i.e., a mean-field temperature exponent ν=1/2) described the results very well [lines in inset of Figure 3(a)]. Compared to initial results from neutron scattering, the superior momentum resolution of IXS allowed an unambiguous determination of the renormalized phonon dispersion, particularly at momenta close to q=0. Moreover, the IXS results were not limited by

weak signals from too small samples. Combined with previous measurements of the uniform nematic susceptibility χ_{nem}, the IXS experiments showed that two independent critical exponents γ=1 (for χ_{nem}) and ν=1/2 (for ξ) are those of a mean-field critical point.

IXS experiments in the hole-doped Ba$_{1-x}$(K,Na)$_x$Fe$_2$As$_2$ and Sr$_{1-x}$Na$_x$Fe$_2$As$_2$ revealed a different scenario [95]. Here, magnetic ordering and structural distortion occur simultaneously, and no nematic phase (without long-range magnetic order) exists. IXS experiments showed that the correlation length of nematic fluctuations ξ above T$_s$ (= T$_N$) in optimally hole-doped compounds ($\xi < 53$Å) is significantly shorter than in the Co-doped system ($\xi > 100$Å) [95]. The small correlation length allows a straightforward determination of the corresponding elastic constant(s) from the IXS experiments at small wave vectors. This was particularly interesting for underdoped Ba$_{0.735}$Na$_{0.265}$Fe$_2$As$_2$ and Sr$_{0.67}$Na$_{0.33}$Fe$_2$As$_2$, in which the transition to an orthorhombic structure at T$_s$ is followed by the transition to a re-entrant tetragonal but magnetically ordered phase at T$_1$ < T$_s$. Entering or exiting the orthorhombic phase, typical techniques for the determination of elastic constants such as ultrasound or three-point bending measurements are affected by twinning [92–94]. Hence, the results derived from IXS [95] represent the first reliable determination of the elastic constants across these intriguing phase transitions. A comparison between the results from IXS (symbols) and 3-point bending measurements (line) are shown in Figure 3(b). The minimum of C$_{66}$ in the magnetically ordered tetragonal phase for both Ba$_{0.735}$Na$_{0.265}$Fe$_2$As$_2$ and Sr$_{0.67}$Na$_{0.33}$Fe$_2$As$_2$ [95] suggests a large low-temperature nematic susceptibility.

Nickel-based superconductors: Soft phonons and CDW formation

New insights in the interplay between nematicity, charge ordering, and superconductivity have been offered by recent experiments on a Ni-based family of compounds, with BaNi$_2$As$_2$ being its parent member [96–102]. BaNi$_2$As$_2$ shares the same room-temperature structure with BaFe$_2$As$_2$, the parent compound of the Fe-based superconductors, and is often viewed as its non-magnetic homologue. At a lower temperature (T$_s$=135 K), the system undergoes a first-order phase transition towards a triclinic structure and becomes superconducting below T$_c$=0.7 K [103]. Magnetic ordering has not been observed, neither in the tetragonal nor in the triclinic phase. Instead, an incommensurate charge density wave (I-CDW) has been observed in the high-temperature tetragonal phase of BaNi$_2$As$_2$ [100] and has been associated with electronic nematicity in a similar manner to that of magnetic ordering in the iron-based superconductors, albeit in the charge channel [99].

Central to this analogy with the iron-based relatives stood the observed I-CDW satellites in X-ray diffraction experiments, which form a "square" pattern, questioning whether the I-CDW is intrinsically uniaxial or not [98, 100, 104]. Recent IXS experiments in BaNi$_2$As$_2$, in combination with density functional perturbation theory (DFPT) calculations, clarified that the I-CDW order in this system is driven by the complete softening of a transversely polarized optical phonon mode (see Figure 4(b)) [105, 106]. The I-CDW satellites appear at the recip-
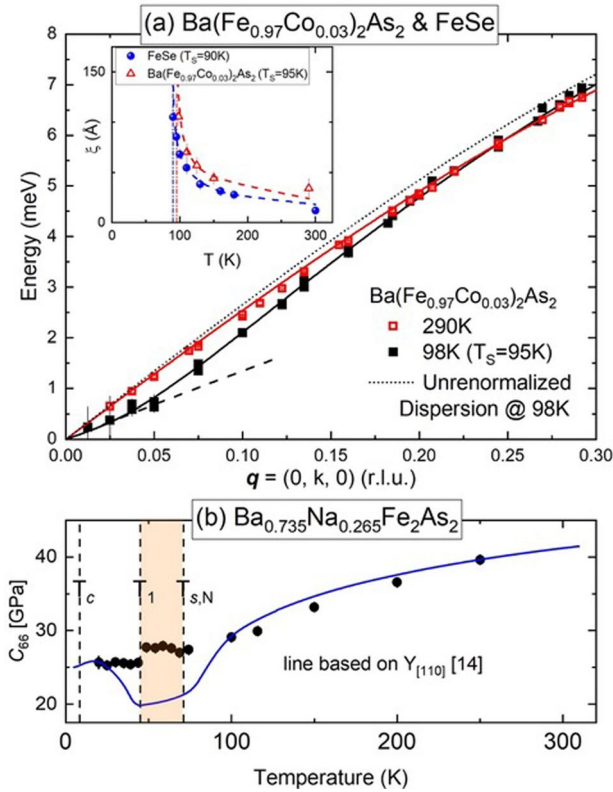

Figure 3: (a) Renormalized dispersion of the TA soft mode in Ba(Fe$_{0.97}$Co$_{0.03}$)$_2$As$_2$. The dotted line represents the unrenormalized dispersion. Solid lines denote the approximated model dispersion given in Eq. (1). The inset shows the temperature dependence of the deduced nematic correlation length for Ba(Fe$_{0.97}$Co$_{0.03}$)$_2$As$_2$ and FeSe. Reprinted figure with permission from [87]. Copyright (2020) by the American Physical Society. (b) Temperature-dependent shear modulus C$_{66}$ deduced from IXS experiments (symbols) compared to results based on measurements of the Young's modulus Y$_{[110]}$ (line [94]). Reprinted figure with permission from [95]. Copyright (2020) by the American Physical Society.
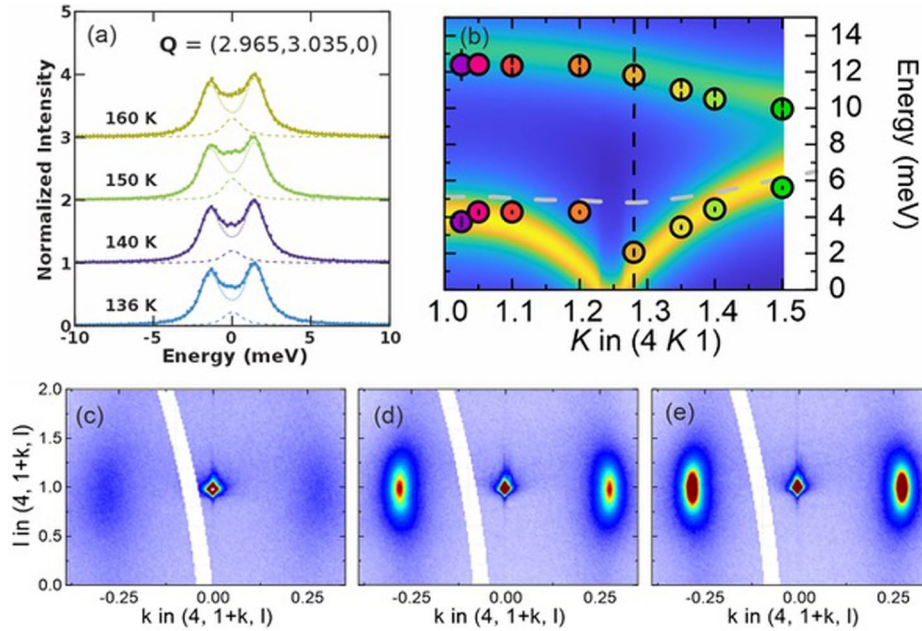
Figure 4: (a, b) Temperature evolution of the IXS spectra of $BaNi_2As_2$ measured at Q = (3 + q, 3 – q, 0) with q = 0.035, dominated by in-plane transversely polarized acoustic phonons. Reprinted figure with permission from [105]. Copyright (2023) by the American Physical Society. (b) Dispersion of the phonons of $BaNi_2As_2$ measured close to the (411) Bragg reflection and along the [0k0] direction at 250 K. The colormap depicts the scattering intensity as calculated by DFPT. Reprinted figure with permission from [106]. Copyright (2022) by the American Physical Society. (d-f) Intensity maps of the 4KL reciprocal lattice plane of $BaNi_2As_2$ reconstructed from DS data collected at (d) 293, (e) 154, and (f) 139 K. Reprinted figures with permission from [106]. Copyright (2022) by the American Physical Society.

rocal space positions where the soft transverse phonon branch is probed, providing a simple explanation for their observed pattern and settling the unidirectional nature of the I-CDW [106]. This is, for instance, illustrated in Figure 4(c)–(e), in which DS signal related to the CDW soft phonon mode is observed at incommensurate positions around the main Bragg, but only along the transverse direction. The momentum span of the DS signal along the different directions can be directly translated in the respective correlation lengths of the I-CDW. Its temperature dependence—which, due to the significantly shorter DS measurement times, can be explored in much finer steps compared to the one of IXS spectra—showed that the divergence of the correlation length coincides with the appearance of a small orthorhombic distortion seen in dilatometry experiments [101]. This indicates that the breaking of the C_4 rotational symmetry is a by-product of the formation of the long-range I-CDW order and calls for additional investigations regarding the parallelism to the case of the iron-based superconductors.

Along this direction, IXS measurements of the dispersion of in-plane transverse acoustic phonons at small wavevectors have been performed to explore the coupling between nematicity and the lattice in the B_{1g} channel, for which the elastoresistance was shown to be enhanced when approaching the structural transition [105]. Unlike the case of the iron-based superconductors though, for several members of

which a clear phonon softening was observed as outlined earlier, the energy of the acoustic phonons in $BaNi_2As_2$ did not exhibit any clear temperature dependence that could be linked to nematicity (Figure 4(a)). This indicates that the enhancement of the B_{1g} elastoresistance close to the structural transition is not driven by the lattice [99, 102]. Currently, there are no reports on the behavior of the phonons on chemically substituted $BaNi_2As_2$ samples, for which a large increase of the superconducting T_c has been observed and linked to the strengthening of nematic fluctuations [99].

Summary and outlook

Competing orders are encountered more often than not in the phase diagrams of unconventional superconductors, attributing a particular importance to the understanding of their origin and interplay. Phonons and their coupling to the electrons, being either the main driving force or simply a spectator, can serve as valuable probes of this interplay, typically achieved by monitoring renormalizations of the phonon spectra when different types of electronic orders set in. The studies presented in this report give a short overview of recent contributions of phonon X-ray spectroscopy in this field, in three different families of unconventional superconductors for which superconductivity appears in close proximity to charge order, magnetism, and electronic nematicity. Technical advances in synchrotron light sources and X-ray scattering beamlines—in particular, higher incident

X-ray flux, reduced incident beam dimensions, and advanced sample environment capabilities—will be within reach in the foreseeable future and will elucidate further the landscape of competing orders in unconventional superconductors.

ORCID

S. M. Souliou http://orcid.org/0000-0001-9201-7392
F. Weber http://orcid.org/0000-0002-4256-1354
M. Le Tacon http://orcid.org/0000-0002-5838-3724

References

1. M. R. Norman, *Science.* **332** (6026), 196 (2011). doi:10.1126/science.1200181.
2. J. Bardeen, L. N. Cooper, and J. R. Schrieffer, *Phys. Rev.* **108** (5), 1175 (1957).
3. E. Fradkin, S. A. Kivelson, and J. M. Tranquada, *Rev. Mod. Phys.* **87** (2), 457 (2015).
4. R. M. Fernandes, P. P. Orth, and J. Schmalian, *Annu. Rev. Condens. Matter Phys.* **10** (1), 133 (2019). doi:10.1146/annurev-conmatphys-031218-013200.
5. Baron, A.Q. (2016). High-Resolution Inelastic X-Ray Scattering I: Context, Spectrometers, Samples, and Superconductors. In: Jaeschke, E., Khan, S., Schneider, J., Hastings, J. (eds) Synchrotron Light Sources and Free-Electron Lasers. Springer, Cham. doi:10.1007/978-3-319-14394-1_41.
6. B. Keimer et al., *Nature.* **518** (7538), 179 (2015). doi:10.1038/nature14165.
7. L. Pintschovius et al., *Phys. Rev. Lett.* **89** (3), 037001 (2002). doi:10.1103/PhysRevLett.89.037001.
8. H. A. Mook et al., *Nature.* **404** (6779), 729 (2000). doi:10.1038/35008005.
9. M. Raichle et al., *Phys. Rev. Lett.* **107** (17), 177004 (2011).
10. D. Reznik et al., *Nature.* **440** (7088), 1170 (2006). doi:10.1038/nature04704.
11. S. R. Park et al., *Phys. Rev. B.* **84** (21), 214516 (2011). doi:10.1103/PhysRevB.84.214516.
12. J. Graf et al., *Phys. Rev. Lett.* **100** (22), 227002 (2008). doi:10.1103/PhysRevLett.100.227002.
13. H. Uchiyama et al., *Phys. Rev. Lett.* **92** (19), 197005 (2004). doi:10.1103/PhysRevLett.92.197005.
14. M. d'Astuto et al., *Phys. Rev. Lett.* **88** (16), 167002 (2002). doi:10.1103/PhysRevLett.88.167002.
15. S. A. Kivelson et al., *Rev. Mod. Phys.* **75** (4), 1201 (2003).
16. D. Reznik, *Physica. C.* **481**, 75 (2012). doi:10.1016/j.physc.2012.01.024
17. G. Ghiringhelli et al., *Science.* **337** (6096), 821 (2012). doi:10.1126/science.1223532
18. T. Wu et al., *Nature.* **477** (7363), 191 (2011). http://www.nature.com/nature/journal/v477/n7363/abs/nature10345.html#supplementary-information. doi:10.1038/nature10345
19. T. Wu et al., *Nat. Comm.* **6**, 6438 (2015). doi:10.1038/ncomms7438.
20. J. Chang et al., *Nature Phys.* **8** (12), 871 (2012). http://www.nature.com/nphys/journal/v8/n12/abs/nphys2456.html#supplementary-information. doi:10.1038/nphys2456
21. M. Hücker et al., *Phys. Rev. B.* **83** (10), 104506 (2011).
22. S. Blanco-Canosa et al., *Phys. Rev. B.* **90** (5), 054513 (2014).
23. M. Hücker et al., *Phys. Rev. B.* **90** (5), 054514 (2014).
24. K.-P. Bohnen, R. Heid, and M. Krauss, *Europhys. Lett.* **64** (1), 104 (2003).
25. M. Le Tacon et al., *Nature Phys.* **10** (1), 52 (2014). doi:10.1038/nphys2805.
26. A. Bosak et al., *J. Phys. D: Appl. Phys.* **48** (50), 504003 (2015). doi:10.1088/0022-3727/48/50/504003.
27. H.-H. Kim et al., *Science.* **362** (6418), 1040 (2018). doi:10.1126/science.aat4708
28. S. M. Souliou et al., *J. Phys. Soc. Jpn.* **90** (11), 111006 (2021). doi:10.7566/JPSJ.90.111006.
29. W. S. Lee et al., *Nat. Phys.* **17** (1), 53 (2021). doi:10.1038/s41567-020-0993-7.
30. E. Blackburn et al., *Phys. Rev. B.* **88** (5), 054506 (2013). doi:10.1103/PhysRevB.88.054506.
31. S. M. Souliou et al., *Phys. Rev. B.* **97** (2), 020503 (2018). doi:10.1103/PhysRevB.97.020503.
32. H. Miao et al., *Phys. Rev. X.* **8** (1), 011008 (2018).
33. A. Bosak et al., *Phys. Rev. Res.* **3** (3), 033020 (2021). doi:10.1103/PhysRevResearch.3.033020.
34. B. Renker et al., *Phys. Rev. Lett.* **32** (15), 836 (1974).
35. B. Renker et al., *Phys. Rev. Lett.* **30** (22), 1144 (1973).
36. M. Hoesch et al., *Phys. Rev. Lett.* **102** (8), 086402 (2009).
37. Y.-H. Liu et al., *Nat. Commun.* **7** (1), 10378 (2016). doi:10.1038/ncomms10378.
38. S. Sarkar, M. Grandadam, and C. Pépin, *Phys. Rev. Res.* **3** (1), 013162 (2021). doi:10.1103/PhysRevResearch.3.013162.
39. R. Arpaia et al., *Science.* **365** (6456), 906 (2019). doi:10.1126/science.aav1315.
40. L. J. P. Ament et al., *Rev. Mod. Phys.* **83** (2), 705 (2011).
41. Y. Y. Peng et al., *Phys. Rev. Lett.* **125** (9), 097002 (2020). doi:10.1103/PhysRevLett.125.097002.
42. H. Miao et al., *Phys. Rev. X.* **9** (3), 031042 (2019). doi:10.1103/PhysRevX.9.031042.
43. T. P. Devereaux et al., *Phys. Rev. X.* **6** (4), 041019 (2016).
44. M. Rossi et al., *Phys. Rev. Lett.* **123** (2), 027001 (2019). doi:10.1103/PhysRevLett.123.027001.
45. L. Chaix et al., *Nature Phys.* **13** (10), 952 (2017). doi:10.1038/nphys4157.
46. A. P. Drozdov et al., *Nature.* **569** (7757), 528 (2019). doi:10.1038/s41586-019-1201-8.
47. A. P. Drozdov et al., *Nature.* **525** (7567), 73 (2015). doi:10.1038/nature14964.
48. S. M. Souliou et al., *Supercond. Sci. Technol.* **33** (12), 124004 (2020). doi:10.1088/1361-6668/abbdc3.
49. S. Sadewasser et al., *Phys. Rev. B.* **61** (1), 741 (2000). doi:10.1103/PhysRevB.61.741.
50. A. C. Mark, J. C. Campuzano, and R. J. Hemley, *High Pressure Res.* **42** (2), 137 (2022). doi:10.1080/08957959.2022.2059366.
51. C. Putzke et al., *Phys. Rev. Lett.* **120** (11), 117002 (2018). doi:10.1103/PhysRevLett.120.117002.
52. I. Vinograd et al., *Phys. Rev. B.* **100** (9), 094502 (2019). doi:10.1103/PhysRevB.100.094502.
53. H. Alloul et al., *Rev. Mod. Phys.* **81** (1), 45 (2009).
54. S. Blanco-Canosa et al., *Phys. Rev. Lett.* **110** (18), 187001 (2013). doi:10.1103/PhysRevLett.110.187001.
55. M. Le Tacon et al., *Phys. Rev. B.* **76** (14), 144505 (2007). doi:10.1103/PhysRevB.76.144505.
56. M. Limonov et al., *Phys. Rev. B.* **65** (2), 024515 (2001).

57. Y. Fukuzumi, K. Mizuhashi, and S. Uchida, *Phys. Rev. B.* **61** (1), 627 (2000). doi:10.1103/PhysRevB.61.627.

58. G. Grissonnanche et al., *Nat. Comm.* **5**, 3280 (2014). doi:10.1038/ncomms4280.

59. O. Kraut et al., *Physica C.* **205** (1-2), 139 (1993). doi: 10.1016/0921-4534(93)90180-X

60. M. Frachet et al., *Phys. Rev. B.* **105** (4), 045110 (2022). doi:10.1103/PhysRevB.105.045110.

61. M. E. Barber et al., *Phys. Rev. B.* **106** (18), 184516 (2022). doi:10.1103/PhysRevB.106.184516.

62. H. H. Kim et al., *Phys. Rev. Lett.* **126** (3), 037002 (2021). doi:10.1103/PhysRevLett.126.037002.

63. H. Jang et al., *Proc. Natl. Acad. Sci. USA.* **113** (51), 14645 (2016). doi:10.1073/pnas.1612849113.

64. S. Gerber et al., *Science.* **350** (6263), 949 (2015). doi:10.1126/science.aac6257.

65. J. Kačmarčík et al., *Phys. Rev. Lett.* **121** (16), 167002 (2018). doi:10.1103/PhysRevLett.121.167002.

66. F. Laliberté et al., *Npj Quant. Mater.* **3** (1), 11 (2018). doi:10.1038/s41535-018-0084-5.

67. D. LeBoeuf et al., *Nature Phys.* **9** (2), 79 (2013). http://www.nature.com/nphys/journal/v9/n2/abs/nphys2502.html#supplementary-information. doi:10.1038/nphys2502

68. P. Dai, *Rev. Mod. Phys.* **87** (3), 855 (2015). doi:10.1103/RevModPhys.87.855.

69. D. C. Johnston, *Adv. Phys.* **59** (6), 803 (2010). doi:10.1080/00018732.2010.513480.

70. S. Nandi et al., *Phys. Rev. Lett.* **104** (5), 057006 (2010). doi:10.1103/PhysRevLett.104.057006.

71. A. E. Böhmer et al., *Nat. Commun.* **6** (1), 7911 (2015). doi:10.1038/ncomms8911.

72. S. Avci et al., *Phys. Rev. B.* **85** (18), 184507 (2012). doi:10.1103/PhysRevB.85.184507.

73. E. P. Rosenthal et al., *Nature Phys.* **10** (3), 225 (2014). doi:10.1038/nphys2870.

74. S. Hosoi et al., *Proc. Natl. Acad. Sci. USA.* **113** (29), 8139 (2016). doi:10.1073/pnas.1605806113.

75. M. Le Tacon et al., *J. Phys. Chem. Solids* **72** (5), 523 (2011). doi:10.1016/j.jpcs.2010.10.006.

76. M. Le Tacon et al., *Phys. Rev. B.* **80** (22), 220504 (2009). doi:10.1103/PhysRevB.80.220504.

77. M. Le Tacon et al., *Phys. Rev. B.* **78** (14), 140505 (2008). doi:10.1103/PhysRevB.78.140505.

78. Y. Kamihara et al., *J. Am. Chem. Soc.* **130** (11), 3296 (2008). doi:10.1021/ja800073m.

79. D. Reznik et al., *Phys. Rev. B.* **80** (21), 214534 (2009). doi:10.1103/PhysRevB.80.214534

80. T. Fukuda et al., *J. Phys. Soc. Jpn.* **77** (10), 103715 (2008). doi:10.1143/JPSJ.77.103715.

81. T. Fukuda et al., *Phys. Rev. B.* **84** (6), 064504 (2011). doi:10.1103/PhysRevB.84.064504.

82. N. Murai et al., *Phys. Rev. B.* **93** (2), 020301 (2016). doi:10.1103/PhysRevB.93.020301.

83. D. Lamago et al., *Phys. C-Superconduct. Appl.* **471** (23–24), 1595 (2011). doi:10.1016/j.physc.2011.08.004.

84. J. L. Niedziela et al., *Phys. Rev. B.* **84** (22), 224305 (2011). doi:10.1103/PhysRev.B.84.224305.

85. D. Parshall et al., *Phys. Rev. B.* **91** (13), 134426 (2015). doi:10.1103/PhysRevB.91.134426.

86. F. Weber et al., *Phys. Rev. B.* **98** (1), 014516 (2018). doi:10.1103/PhysRevB.98.014516.

87. A. M. Merritt et al., *Phys. Rev. Lett.* **124** (15), 157001 (2020). doi:10.1103/PhysRevLett.124.157001.

88. H. H. Kuo et al., *Science.* **352** (6288), 958 (2016). doi:10.1126/science.aab0103.

89. A. E. Böhmer, and C. Meingast, *CR. Phys.* **17** (1-2), 90 (2016). doi:10.1016/j.crhy.2015.07.001.

90. R. M. Fernandes, A. V. Chubukov, and J. Schmalian, *Nature Phys.* **10** (2), 97 (2014). doi:10.1038/nphys2877.

91. R. M. Fernandes et al., *Phys. Rev. Lett.* **105** (15), 157003 (2010).

92. A. E. Böhmer et al., *Phys. Rev. Lett.* **112** (4), 047001 (2014). doi:10.1103/PhysRevLett.112.047001.

93. M. Yoshizawa et al., *J. Phys. Soc. Jpn.* **81** (2), 024604 (2012).

94. L. Wang et al., *Phys. Rev. B.* **97** (22), 224518 (2018). doi:10.1103/PhysRevB.97.224518.

95. M. Kauth et al., *Phys. Rev. B.* **102** (14), 144526 (2020). doi:10.1103/PhysRevB.102.144526.

96. A. R. Pokharel et al., *Commun. Phys.* **5** (1), 141 (2022). doi:10.1038/s42005-022-00919-x.

97. Y. Yao et al., *Nat. Comm.* **13** (1), 4535 (2022). doi:10.1038/s41467-022-32112-7.

98. S. Lee et al., *Phys. Rev. Lett.* **127** (2), 027602 (2021). doi:10.1103/PhysRevLett.127.027602.

99. C. Eckberg et al., *Nat. Phys.* **16** (3), 346 (2020). doi:10.1038/s41567-019-0736-9.

100. S. Lee et al., *Phys. Rev. Lett.* **122** (14), 147601 (2019). doi:10.1103/PhysRevLett.122.147601.

101. C. Meingast et al., *Phys. Rev. B.* **106** (14), 144507 (2022). doi:10.1103/PhysRevB.106.144507.

102. M. Frachet et al., *Npj Quantum Mater.* **7** (1), 115 (2022). doi:10.1038/s41535-022-00525-8.

103. F. Ronning et al., *J. Phys: Condens. Matter.* **20** (34), 342203 (2008). doi:10.1088/0953-8984/20/34/342203.

104. M. Merz et al., *Phys. Rev. B.* **104** (18), 184509 (2021). doi:10.1103/PhysRevB.104.184509.

105. Y. Song et al., *Phys. Rev. B.* **107** (4), L041113 (2023). doi:10.1103/PhysRevB.107.L041113.

106. S. M. Souliou et al., *Phys. Rev. Lett.* **129** (24), 247602 (2022). doi:10.1103/PhysRevLett.129.247602.